# Vortex Formation and Annihilation in Three Textures of Rotating Superfluid $^3$He-*A*

R. Ishiguro,[2] O. Ishikawa,[3] M. Yamashita,[2] Y. Sasaki,[2,4] K. Fukuda,[5] M. Kubota,[1] H. Ishimoto,[1] R. E. Packard,[6] T. Takagi,[7] T. Ohmi,[2] and T. Mizusaki[1,2,4]

[1]*Institute for Solid State Physics, University of Tokyo, Chiba 277-8581, Japan*
[2]*Department of Physics, Graduate School of Science, Kyoto University, Kyoto 606-8502, Japan*
[3]*Graduate School of Science, Osaka City University, Osaka 558-8585, Japan*
[4]*Research Center for Low Temperature and Materials Sciences, Kyoto University, Kyoto 606-8502, Japan*
[5]*College of Medical Technology, Kyoto University, Kyoto 606-8507, Japan*
[6]*Department of Physics, University of California, Berkeley, California 94720, USA*
[7]*Department of Applied Physics, Fukui University, Fukui 910-8507, Japan*
(Received 5 March 2003; published 17 September 2004)

Textures, textural transformation, and formation and annihilation of a single vortex were investigated in narrow cylinders with 100 $\mu$m radius in *A*-phase under rotation up to 6.28 rad/sec. Three textures were found, depending on the cooling conditions of the sample through the superfluid transition temperature $T_c$. We found the gyromagnetic effect of textures; that is, two textures (*A* or *B*) could be selected either by applying a magnetic field in parallel or anti-parallel to the rotation axis. The critical angular speed of a single vortex formation $\Omega_f$ and that of annihilation $\Omega_a$ for each texture were measured. The textural transformation in type *A* texture was induced by rotation. Both type *A* and *B* textures held macroscopic angular momentum along the rotation axis. We identified the texture for type *A*, *B*, and *C* as Mermin-Ho, radial disgyration, and a soliton type of defect along the axis, respectively.

DOI: 10.1103/PhysRevLett.93.125301 PACS numbers: 67.57.Fg, 47.32.–y

Vortices in the bulk superfluid $^3$He-*A* phase were studied extensively [1,2], including their nucleation and annihilation at a wall [3–5] and at the *A*-*B* phase boundary [6]. However, the behavior of a single vortex in this system was studied only recently [7]. To further our understanding of the vortex transition process, we constructed a new rotating cryostat [8] which can rotate up to 6.28 rad/sec, a speed sufficient to create a vortex in the restricted geometry of a narrow tube. This allowed us to study single vortex formation and texture transformation due to flow in a well-controlled texture.

Earlier measurements in the restricted geometry of a 0.5 mm diameter tube were not conclusive to show either texture transformations or vortex formation under rotation [9]. In a preliminary report [10], we described two types of textures, but could not control them by various cooling conditions. In this Letter, we report success in controlling the textures, thus enabling us to study what kind of *A* phase textures exists in narrow cylinders for various conditions of rotation, magnetic field, and cooling conditions. We can also determine how the texture influences the formation and annihilation of a vortex.

The *A* phase of superfluid $^3$He is described by two vectors. $\hat{\mathbf{l}}$ is a vector specifying the orbital part of the order parameter and $\hat{\mathbf{d}}$ specifies the spin part. A texture refers to the spatial distribution of both vectors in a given sample. Three types of textures have been proposed for a cylindrical geometry: the Mermin-Ho (MH), the Pan-Am (PA), and the radial disgyration (RD) [11,12]. The MH texture has a three-dimensional structure of $\hat{\mathbf{l}}$ producing a circulation of a single quanta $\kappa_0$ ($\kappa_0 = 0.066$ mm$^2$/sec), thus holding a macroscopic angular momentum [12]. The PA texture is planar and does not give rise to macroscopic angular momentum. Finally, the RD texture may possess macroscopic angular momentum even though it has a planar structure because a single quantum of circulation can be attached to the singular core.

We have studied rotating $^3$He-*A* at 31.5 bars in narrow cylinders. The radius of a long narrow cylinder was 100 $\mu$m, which was about 10 times the dipole coherence length $\xi_D$. The sample cell was composed of a bundle of 150 cylinders, both sides of which were connected with bulk liquid $^3$He. The rotation vector was parallel to the cylinder's axis. For our maximum speed of rotation $\Omega = 6.28$ rad/sec, the radius of cylinders was comparable to the spacing in a vortex lattice of doubly-quantized vortex and only a couple of vortex formation is expected.

We performed cw-NMR measurements at 700 kHz, and the NMR magnetic field of about 22 mT was applied parallel to the axis of the cylindrical sample. Regarding the NMR spectrum, vortices and textures may produce spin wave satellite peaks on the widespread background of the textural local mode spectrum. Spin waves are characterized by their normalized frequency shift $R_t^2$, which is related with the resonance frequency $f_0 + R_t^2(f_L^A)^2/2f_0$, where $f_0$ is the Larmor frequency and $f_L^A$ is the temperature-dependent longitudinal frequency in *A* phase. Roughly speaking, the spin wave satellite signal comes from the part of the texture whose spatial variation occurs in the scale of $\xi_D$, while the local mode of spectrum comes from the part which changes slowly in space.

Figure 1 shows three types of cw-NMR absorption spectra, *A* (dotted line), *B* (dashed line), and *C* (solid

  

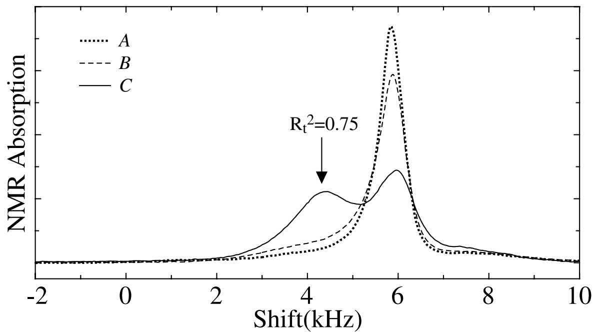


FIG. 1. NMR absorption spectra for $\Omega = 0$ at $T/T_c = 0.75$ as a function of frequency shift from the Larmor frequency. Spectra for three textures, labeled by a dotted line for $A$, a dashed line for $B$, and a solid line for $C$ are shown. Textures were controlled by the condition of cooling through $T_c$.

line), observed at $\Omega = 0$ and $T/T_c = 0.75$, right after it cooled through $T_c$ from a normal phase and stayed in the supercooled $A$ phase. Both types $A$ and $B$ were observed when the liquid was cooled slowly through $T_c$ from normal fluid by a cooling speed of about 1 $\mu$K/min under rotation and then brought to rest. The difference between type $A$ and type $B$ comes from the relative orientation between the magnetic field and the rotation direction while cooling through $T_c$. Type $A$ was created when it was cooled under a rotation speed of $\Omega_{\mathrm{ini}} = +2$ rad/sec with the magnetic field of $-22$ mT. Type $B$ was created when it was cooled under the same rotation speed with the opposite direction of the magnetic field ($+2$ rad/sec, $+22$ mT). The positive directions of the rotation and the magnetic field were chosen to be the upward direction of the sample cell. These spectra look similar to each other but responses to rotation and a formation of vortex were quite different, as described later.

The characteristic features of the spectra for type $A$ and $B$ are that the main peak occurs at $R_t^2 = 1$ and the spectra continuously extended toward $f_0$. The main peak comes from the part of texture with $\hat{\mathbf{l}}//\hat{\mathbf{d}}$. The small peak on the right-hand side of the main peak is the signal from a bulk $A$ phase outside the cylinders, which was shifted due to a finite field gradient of NMR magnet. Type $B$ had a smaller main peak than type $A$ and type $B$ spectrum was broadened to lower frequencies.

Type $C$ was created when the liquid was cooled rapidly through $T_c$ at a cooling rate of about 10 $\mu$K/min without depending on whether it was cooled under rotation or in magnetic field. This texture was also created when the sample was suddenly heated so as not to exceed $T_c$. The main peak height was smaller than other two types, while the large satellite signal appeared at $R_t^2 = 0.75$. This texture was so stable that the same spectrum was observed for a couple of days when the sample was left at rest. However, the satellite peak sometimes became smaller when we created vortices in the sample or rapidly changed the temperature even below $T_c$. This instability of an intensity against external disturbance, the value $R_t^2 = 0.75$, the large satellite intensity, and the one-dimensional NMR imaging of the texture indicated that this satellite signal should come from a soliton-type of planar defect, which extends along the sample cell axis. This texture might be created by the thermal counterflow due to heat input, which flowed parallel to the sample axis. We believe that this was the texture we observed in the previous report (the dotted curve in Fig. 2 in Ref. [13]) according to the spectrum and the way of cooling through $T_c$.

Figure 2 shows typical NMR absorption spectra for the type $A$ at $T/T_c = 0.75$ with increasing rotation speeds. The spectrum at $\Omega = 0$ rad/sec (dotted line) is almost the same as that at $\Omega = 4.0$ rad/sec (solid line). The major change of the NMR spectrum occurred only at around $\Omega_f = 4.8$ rad/sec (dashed line), above which the height of the main peak at $R_t^2 = 1$ decreased and the satellite peak at $R_t^2 = 0.31$ appeared. The spectrum at $\Omega = 6.28$ rad/sec (thick solid line) was almost the same as that at $\Omega = 4.8$ rad/sec. The value of $R_t^2 \sim 0.31$ at $T/T_c = 0.75$ and its temperature dependence was very similar to that for the doubly-quantized continuous vortex observed in bulk $^3$He-A [14]. We therefore identify this sudden change of spectrum as a formation of a single doubly-quantized vortex in the cylinder. When the rotation speed decreased after the vortex formation at $\Omega_f$, the satellite peak disappeared at a different critical rotation speed $\Omega_a$. We attributed this sudden change of spectrum to a vortex annihilation.

Similar formation and annihilation of a vortex were observed for the type $B$ texture. The positions of the satellite peaks of the vortices for both types $A$ and $B$ are almost identical. We observed similar formation and annihilation of a vortex for the type $C$ texture as well. The satellite peaks due to vortex formation also appeared at $R_t^2 \sim 0.3$. Since the type $C$ texture was unstable against external disturbance and vortex formation, we did not investigate it thoroughly.

Figure 3 shows the main peak height as a function of a rotation speed $\Omega$ for type $A$ and $B$. Data in Fig. 3(a) were

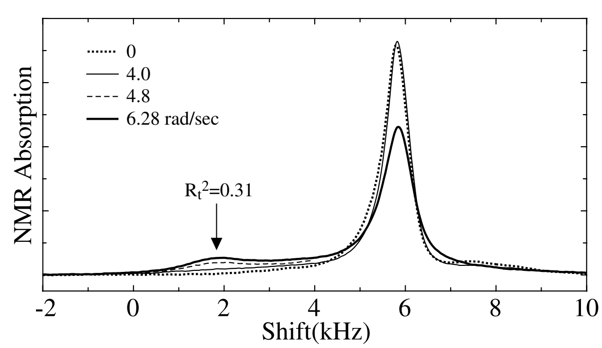


FIG. 2. NMR absorption spectra for type $A$ at $T/T_c = 0.75$ as a function of frequency shift from Larmor frequency with increasing rotation speeds, $\Omega = 0, 4.0, 4.8$, and 6.28 rad/sec. The spin wave peak for a vortex was observed at $R_t^2 = 0.31$.

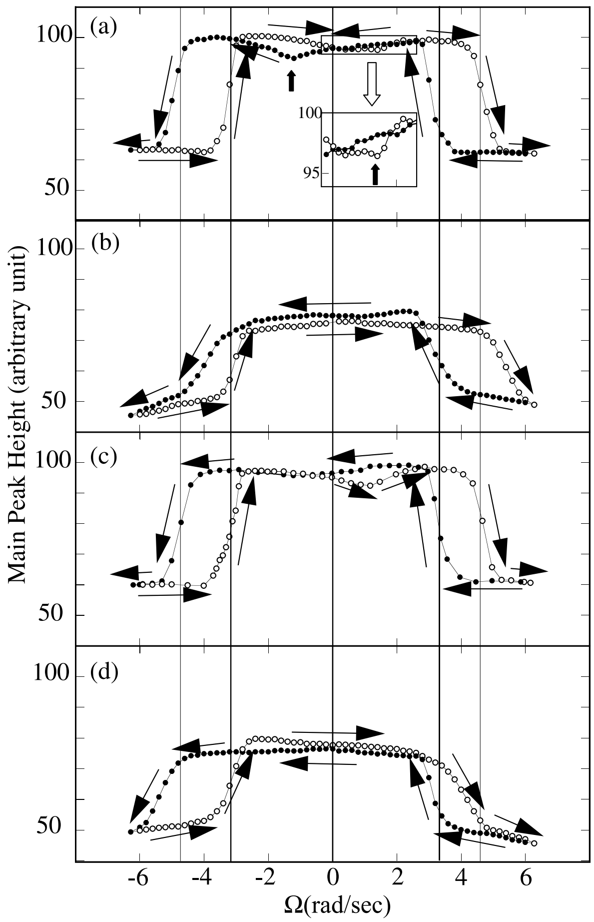


FIG. 3. NMR absorption of the main peak at $R_t^2 = 1.0$ as a function of rotation speed $\Omega$ during acceleration and deceleration cycle. The conditions of cooling the sample though $T_c$ are: (a) (+2 rad/sec, −22 mT), (b) (+2 rad/sec, +22 mT), (c) (−2 rad/sec, +22 mT), (d) (−2 rad/sec, −22 mT). The spectra (a) and (c) correspond to type *A* texture and (b) and (d) to type *B*. Thin arrows indicate the direction of taking data and vertical lines are $\Omega_f$ and $\Omega_a$ for type *A*.

taken for a sample which had been initially cooled through $T_c$ under (+2 rad/sec, −22 mT), whereas data in Fig. 3(c) were taken for a sample cooled under both rotation and field direction simultaneously inverted as (−2 rad/sec, +22 mT). Textures for Figs. 3(a) and 3(c) were identical and classified as type *A*. Data in Fig. 3(b) were taken for a sample cooled through $T_c$ under (+2 rad/sec, +22 mT), whereas data in Fig. 3(d) were for (−2 rad/sec, −22 mT). Textures for Figs. 3(b) and 3(d) were identical and classified as type *B*. The selection between types *A* and *B* was controlled by the relative direction of the magnetic field to rotation direction. Thin arrows indicate the direction of the change of rotation speed. Data were very reproducible and showed a large hysteresis curve between acceleration and deceleration of rotation speed.

As shown in Fig. 3(a), when $\Omega$ increased from $\Omega_{ini} = +2$ rad/sec, a single vortex appeared at $\Omega_f = +4.8$ rad/sec. Here the rotation speed in the middle of a transition was used as the critical rotation speed. When $\Omega$ decreased from +6.28 rad/sec as shown by solid circles, the vortex was annihilated at $\Omega_a = +3.2$ rad/sec. When $\Omega$ further decreased to $\Omega = 0$ and increased in the reversed direction, the big dip shown by the thick arrow appeared at $\Omega_d = -1.5$ rad/sec. When $\Omega$ further increased in the reversed direction, vortex formation occurred at $\Omega_f = -4.8$ rad/sec. Vortex annihilation was observed at $\Omega_a = -3.2$ rad/sec during deceleration. When $\Omega$ decreased to $\Omega = 0$ and increased in the positive direction as shown by open circles, a small dip shown by the thick arrow in the inset of Fig. 3(a) appeared at $\Omega_d = +1.5$ rad/sec. Asymmetry of the size of the dips (not the rotation speed) was also observed in Fig. 3(c), when the sample was cooled with $\Omega_{ini} = -2$ rad/sec. The big dip always appeared in the opposite direction from the initial rotation direction $\Omega_{ini}$. The transition width for both the vortex formation and annihilation was about ±0.5 rad/sec and was attributed to the distribution among the cylinders.

In Figs. 3(b) and 3(d), similar formation and annihilation of a single vortex were observed. But response of type *B* texture against the direction of rotation was not symmetric. The critical rotation speed for annihilation $|\Omega_a|$ was 3.2 rad/sec for both directions and was almost the same as that for type *A*. But the critical speed for formation $|\Omega_f|$ depended on the rotation direction. The $|\Omega_f^+|$ was 5.5 rad/sec for the same rotation direction as the initial rotation direction $\Omega_{ini}$(= ±2 rad/sec). However, $|\Omega_f^-|$ was 4.1 rad/sec for the opposite rotation direction from $\Omega_{ini}$. No dip such as those in type *A* was observed in type *B*. This asymmetry (the dips for type *A* and asymmetric critical speed $|\Omega_f^\pm|$ for type *B*) indicated the asymmetric structure of textures against rotation. Both type *A* and *B* textures should have a macroscopic angular momentum along the rotation axis.

We investigated the temperature dependence of the critical rotation speed $\Omega_f$ and $\Omega_a$. The critical speed $|\Omega_f|$ and $|\Omega_a|$ for type *A*, shown by solid circles and open circles in Fig. 4, did not depend on temperatures up to

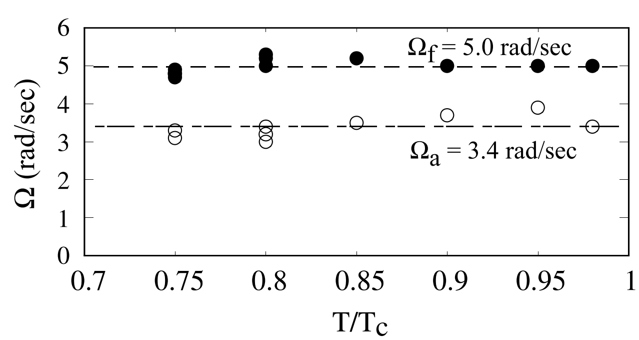


FIG. 4. The critical speed for vortex formation $\Omega_f$ shown by solid circles and annihilation $\Omega_a$ shown by open circles as a function of temperature for type *A* texture.

$T/T_c = 0.975$. The average values, $|\Omega_f| = 5.0$ rad/sec and $|\Omega_a| = 3.4$ rad/sec, are shown by dotted lines. The critical rotation speeds for type $B$, $|\Omega_f^+| = 5.5$ rad/sec, $|\Omega_f^-| = 4.1$ rad/sec, and $|\Omega_a| = 3.2$ rad/sec did not depend on temperature as well.

When the sample was cooled through $T_c$ with $\Omega_{ini} = 4$ rad/sec, a vortex did not appear. Thus, a vortex could not exist in the samples for $\Omega < 4$ rad/sec even at $T_c$. These facts suggest that the observed $\Omega_f$ corresponds to the critical speed $\Omega_{C1}$, which is defined by $F(r, \Omega_{C1}) = F(r) - \Omega_{C1} L_v = 0$ at $r = 0$, where $F(r)$ is the kinetic energy of vortex and $L_v$ is the angular momentum of the vortex, and $r$ is the distance of vortex from the center. The observed $\Omega_a$ can be understood as the critical speed of rotation $\Omega_{CA}$ when the energy barrier for trapped metastable vortex disappears [10,15,16]. These values, $\Omega_{C1}$ and $\Omega_{CA}$, are temperature independent and are comparable to the observed values of $\Omega_f$ and $\Omega_a$, even though we neglected the textural effect [10].

Here we qualitatively discuss the textural effect on $\Omega_f$. If a texture has an angular momentum, $L_t$, the free energy under rotation changes to $F(\Omega) = F - \Omega L_t - \Omega L_v$. Since $L_v$ has the same direction as $\Omega$, the last term is always negative. However, since the sign of $L_t$ depends on the direction of textural angular momentum, the second term changes its sign, depending on the direction of $\Omega$. Thus, a nonzero value of $L_t$ causes the asymmetric response against rotation. The MH texture, MH($\pm$), has a macroscopic angular momentum $L_t$ with a circulation $n = \pm 1$ in the unit of $\kappa_0$ [12]. The RD texture, RD($\pm$), has a singularity at the center, and the circulation of this texture can be $n = \pm 1$ if it is created under a sufficiently high rotation speed. As we have explained earlier, both types $A$ and $B$ texture have a macroscopic angular momentum, which exclude the possibility of PA texture.

We would explain our results in Fig. 3 by identifying type $A$ as MH($\pm$) and type $B$ as RD($\pm$) as follows. For the MH(+) texture in Fig. 3(a), the textural transformation to MH($-$) occurs at the dips when a soft core vortex with $n = -2$ is introduced to the cylindrical sample at $\Omega_d = -1.5$ rad/sec and then two soft cores merge with each other. When the rotation speed increased further in the same direction, a soft core vortex with $n = -2$ is introduced at $\Omega_f = -4.8$ rad/sec and the total circulation becomes $n = -3$. During the deceleration of $\Omega$, a vortex with $n = -2$ disappears at $\Omega_a = -3.2$ rad/sec. And then, another textural transformation from MH($-$) to MH(+) occurs at the dip of $\Omega_d = +1.5$ rad/sec. When $\Omega$ further increases, a soft core vortex with $n = +2$ is introduced at $\Omega_f = +4.8$ rad/sec. Therefore, even though MH texture has a macroscopic angular momentum, the critical velocity of vortex nucleation is symmetric for both rotation directions. This scenario was confirmed by our numerical calculation of the stability of texture with a soft core vortex in cylinder under rotation and will be published elsewhere. We do not know why the depth of the dips is not symmetric for rotation. It should be noted that the spectrum shown in Fig. 2a of Ref. [10] was taken for a sample cooled through $T_c$ without rotation. The textures in this case were considered to be mixtures of MH(+) and MH($-$), hence we did not observe clear dips at $\pm 1.5$ rad/sec. For the RD(+) texture in Fig. 3(b), it is unlikely that the singular vortex core of the RD texture can be merged with a soft core vortex with $n = -2$. Therefore, the RD texture does not transform, even though a soft core vortex is introduced at $\Omega_f^+$ or $\Omega_f^-$. Thus, a vortex formation becomes asymmetric for rotation due to a fixed circulation with $n = \pm 1$.

We have investigated the vortex formation in well-controlled textures in a cylinder. It was surprising that the textures could be controlled by the relative direction between the magnetic field and rotation when the sample was cooled through $T_c$. This is a kind of gyromagnetic effect and further theoretical studies are needed.

This work was carried out using the rotating cryostat at the ISSP, University of Tokyo, and was partially supported by the NSF, the Grant-in-Aid for Scientific Research from MEXT, the U.S.-Japan Cooperative Science Program of the JSPS, and the Grant-in-Aid for the 21st Century COE "Center for Diversity and Universality in Physics."

[1] E. R. Dobbs, *Helium Three* (Oxford University Press, New York, 2000).
[2] O. V. Lounasmaa and E. V. Thuneberg, Proc. Natl. Acad. Sci. U.S.A. **96**, 7760 (1999).
[3] V. M. H. Ruutu *et al.*, Phys. Rev. Lett. **79**, 5058 (1997).
[4] V. M. Ruutu *et al.*, Phys. Rev. B **56**, 14089 (1997).
[5] P. M. Walmsley, D. J. Cousins, and A. I. Golov, Phys. Rev. Lett. **91**, 225301 (2003).
[6] R. Blaauwgeers *et al.*, Phys. Rev. Lett. **89**, 155301 (2002).
[7] R. Blaauwgeers *et al.*, Nature (London) **404**, 471 (2000).
[8] M. Kubota *et al.*, Physica B (Amsterdam) **329-333**, 1577 (2003).
[9] P. J. Hakonen and K. K. Nummila, Jpn. J. Appl. Phys. Part 1, Suppl. **26-3**, 181 (1987).
[10] R. Ishiguro *et al.*, Physica B (Amsterdam) **329-333**, 66 (2003).
[11] D. Vollhardt and P. Wölfle, *The Superfluid Phases of Helium 3* (Taylor & Francis, London, 1990).
[12] N. D. Mermin and Tin-Lun Ho, Phys. Rev. Lett. **36**, 594 (1976).
[13] O. Ishikawa *et al.*, Physica B (Amsterdam) **284-288**, 248 (2000).
[14] V. M. H. Ruutu, Ü. Parts, and M. Krusius, J. Low Temp. Phys. **103**, 331 (1996).
[15] R. E. Packard and T. M. Sanders, Jr., Phys. Rev. A **6**, 799 (1972).
[16] G. B. Hess, Phys. Rev. **161**, 189 (1967).